JOURNAL OF MAGNETIC RESONANCE, Series A 103, 72–81 (1993)

# Pure-Absorption-Mode Lineshapes and Sensitivity in Two-Dimensional Dynamic-Angle Spinning NMR

P. J. GRANDINETTI, J. H. BALTISBERGER, A. LLOR,* Y. K. LEE,† U. WERNER, M. A. EASTMAN, AND A. PINES

*Materials Sciences Division, Lawrence Berkeley Laboratory, 1 Cyclotron Road, Berkeley, California 94720; and Department of Chemistry, University of California, Berkeley, California 94720*

Received September 21, 1992

Modified versions of the *d*ynamic-*a*ngle *s*pinning (DAS) experiment that provide pure-absorption-mode 2D spectra with an increase in sensitivity are described. These new experiments employ time shifting of the coherence-transfer echoes in the DAS experiment, which are formed because of the inhomogeneous broadenings, to acquire both halves of the DAS echo. Optimum 2D time-domain filtering and automated 2D phase-correction techniques relevant to these DAS experiments are also presented. Experimental examples for the central transition of $^{87}Rb$ in polycrystalline $RbClO_4$ and $RbNO_3$ are shown. © 1993 Academic Press, Inc.

## INTRODUCTION

Dynamic-angle spinning (*1–3*) (DAS) removes from the central transition of half-integer quadrupolar nuclei the second-order broadenings that are not removed by magic-angle spinning. In addition, DAS provides a two-dimensional correlation between the isotropic resonance of a quadrupolar spin and its anisotropic lineshape. The high-resolution isotropic dimension provides information on the chemical and second-order quadrupolar shifts, while the separated anisotropic lineshape provides information on the anisotropic spin interaction tensors, such as chemical shift or quadrupolar or heteronuclear dipolar coupling. The anisotropic tensor parameters provide valuable structural information that is not available from a high-resolution isotropic spectrum.

In the original 2D DAS experiments (*2–4*), mixed absorption- and dispersion-mode lineshapes in the two-dimensional DAS spectrum and low signal-to-noise ratios made it difficult to analyze lineshapes in the anisotropic dimension and extract complete spin interaction tensor information. In an earlier work (*5*), we proposed a modification of the DAS pulse sequence that provides pure-absorption-mode 2D DAS spectra by employing a $z$ filter at the end of the first evolution period. This approach has an advantage that the spinner axis may be reoriented during the $z$ filter to the magic angle, where the anisotropic quadrupolar lineshapes are more easily analyzed. The use of additional storage pulses of the $z$-filter approach, however, sacrifices the usual $2^{1/2}$ increase in signal-to-noise of a pure-phase over a mixed-phase 2D spectrum (*6*).

In this paper, we outline some alternative approaches for obtaining pure-absorption-mode 2D DAS spectra that increase the signal-to-noise ratio by up to a factor of $8^{1/2}$ over those of the original (*3*) and $z$ filter (*5*) DAS experiments. In one approach, we redefine the DAS evolution times and apply a corresponding shearing transformation to obtain a pure-absorption-mode 2D DAS spectrum from hypercomplex 2D data. In a second approach we employ a $\pi$ pulse to time shift the coherence-transfer echoes, which are formed because of the angle hop in the DAS experiment, to acquire both halves of the DAS echo signal and obtain a pure-absorption-mode 2D DAS spectrum. In certain circumstances, these two approaches can be combined for an additional increase in sensitivity. In addition, a difficulty with applying an optimum time-domain filter function to hypercomplex 2D data is described, and a method around this difficulty is suggested. A technique for automating the phase correction of 2D DAS spectra using the time-shifted coherence-transfer echo is also presented. The modifications described here should aid in reducing many of the experimental difficulties associated with extracting shift and lineshape information.

## DAS AND SHEARING TRANSFORMATIONS

In the DAS experiment the angle of the rotor axis is switched between two angles $(\theta_1, \theta_2)$ chosen so the dephasing of the signal from anisotropic evolution at $\theta_1$ is completely refocused into an echo during evolution at $\theta_2$. For the central transition of half-integer quadrupolar nuclei broadened to second order, the angle pair $(\theta_1, \theta_2)$ fulfills the conditions

$$x_1 P_2(\cos\theta_1) + x_2 P_2(\cos\theta_2) = 0, \quad [1]$$

$$x_1 P_4(\cos\theta_1) + x_2 P_4(\cos\theta_2) = 0, \quad [2]$$

* Direction des Sciences de la Matière DRECAM/SCM, Commissariat à l'Energie Atomique, Saclay, 91191 Gif-sur-Yvette Cedex, France.

† Health Effects Research Division, Lawrence Berkeley Laboratory, 1 Cyclotron Road, Berkeley, California 94720; and Department of Biophysics, University of California, Berkeley, California 94720.

1064-1858/93 $5.00
Copyright © 1993 by Academic Press, Inc.
All rights of reproduction in any form reserved.

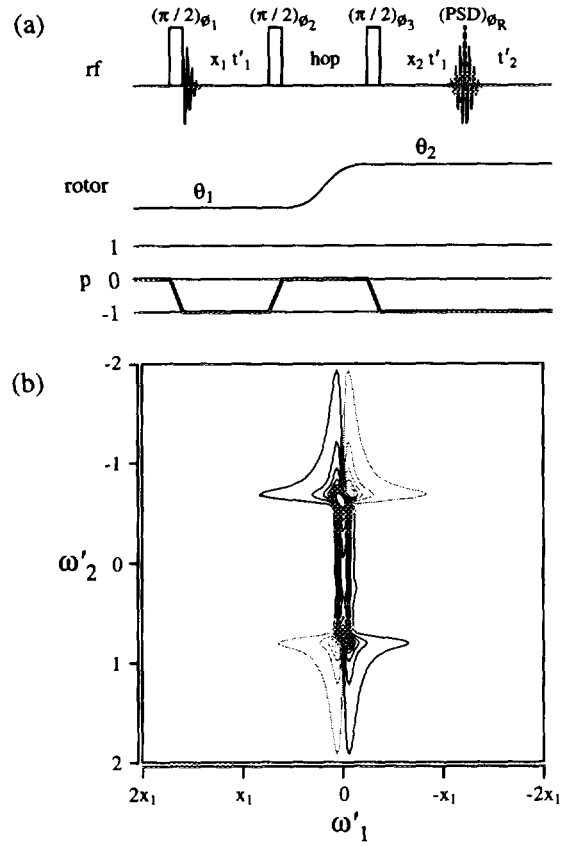


FIG. 1. (a) Pulse sequence for dynamic-angle spinning (DAS) after Llor and Virlet (*1*) and Mueller *et al.* (*3*). (b) Mixed absorption–dispersion-mode 2D DAS lineshape obtained when using the pulse sequence in (a). The contour plot was calculated using 16 equally spaced contour levels over a range of −30 to 70% of the maximum peak. Negative contours are shown in gray.

and

$$x_1 + x_2 = 1, \qquad [3]$$

where $x_1$ and $x_2$ are the fractions of the first evolution time, $t'_1$, spent at each angle. These equations may be solved analytically for the angles $(\theta_1, \theta_2)$ in terms of $x_1$ and $x_2$,

$$\theta_1 = \cos^{-1}\sqrt{\frac{1 + \sqrt{4x_2/5x_1}}{3}}, \qquad [4]$$

$$\theta_2 = \cos^{-1}\sqrt{\frac{1 - \sqrt{4x_1/5x_2}}{3}}, \qquad [5]$$

where $0.8 \leq x_2/x_1 \leq 5$. Of course, the order of the angle pair may be reversed with a corresponding reversal of the fractional time spent at each angle.

In the original DAS experiment, shown in Fig. 1a, only a single coherence-transfer pathway (*7*) is selected, which has the effect of converting the amplitude modulation in $x_1 t'_1$ into phase modulation in order to distinguish positive and negative frequencies during $x_1 t'_1$. In addition, the acquisition is delayed to begin at the echo maximum. This results in a mixture of absorption- and dispersion-mode lineshapes in the 2D DAS spectrum, as exemplified in Fig. 1b.

Although, in the original DAS experiment, the $p = 0 \rightarrow -1 \rightarrow 0 \rightarrow -1$ pathway, commonly referred to as the antiecho pathway, is selected, the sign of the anisotropic broadening reverses during the hop so that an echo-type signal is obtained. To avoid confusion in the following discussion we shall refer to the $p = 0 \rightarrow -1 \rightarrow 0 \rightarrow -1$ and $p = 0 \rightarrow +1 \rightarrow 0 \rightarrow -1$ pathways of the DAS experiment as the echo and antiecho pathways, respectively.

It is well known that in 2D echo experiments like DAS, the evolution times $t'_1$ and $t'_2$ may be redefined so that acquisition begins immediately after the last pulse. The modified DAS pulse sequence shown in Fig. 2a results in a spectrum, as shown in Fig. 2b, that is related to the conventional DAS spectrum by a shearing transformation (*7–13*). This spectrum is a two-dimensional correlation between the one-

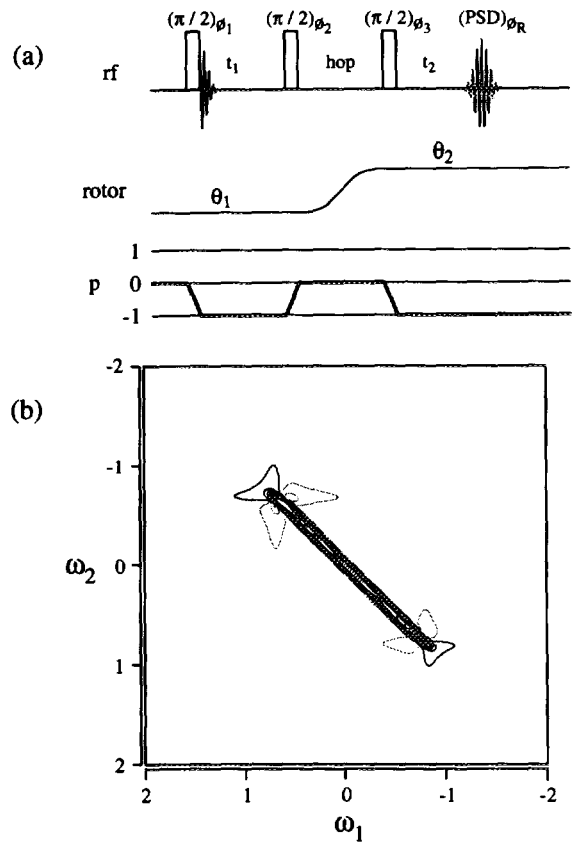


FIG. 2. (a) Modified DAS pulse sequence. (b) Mixed absorption–dispersion-mode 2D DAS lineshape obtained when using the pulse sequence in (a). The contour plot was calculated using 16 equally spaced contour levels over a range of −30 to 70% of the maximum peak. Negative contours are shown in gray. This 2D spectrum is related to the conventional 2D DAS spectrum through a shearing transformation.

dimensional variable-angle spinning (VAS) spectra associated with each rotor angle in the DAS experiment. The shearing transformation may be implemented by applying a $t_1$-dependent first-order phase correction,

$$S'(t_1', \omega_2') = e^{i\phi(t_1,\omega_2)} S(t_1, \omega_2), \qquad [6]$$

where

$$\phi(t_1, \omega_2) = \frac{x_2}{x_1}\omega_2 t_1, \qquad [7]$$

before the final Fourier transform with respect to $t_1'$. This correction removes the tilting in $S(\omega_1, \omega_2)$, transforming it into $S'(\omega_1', \omega_2')$, so that an isotropic spectrum may be obtained from a projection onto the $\omega_1'$ axis.

While the sequences in Figs. 1a and 2a both result in mixed-phase 2D spectra, the dispersion-mode components in Fig. 2b have less intensity than those in Fig. 1b. This is a consequence of the inhomogeneous broadenings inherent in the DAS experiment. In one of the approaches in the next section, we exploit this behavior to eliminate dispersion components in 2D DAS spectra.

## PURE-ABSORPTION-MODE LINESHAPES IN DAS

### *Hypercomplex DAS*

The modified DAS experiment of Fig. 2a may be viewed as a 2D exchange experiment (*7*) with a rotor reorientation during the mixing time, and, as in the 2D exchange experiment, an amplitude-modulated response in $t_1$ makes it possible to obtain pure-absorption-mode 2D spectra using the hypercomplex (*7, 14*) or TPPI (*15*) approach to 2D data acquisition. The pulse sequence and phase cycle for the hypercomplex approach to pure-phase DAS are described in Fig. 3. The hypercomplex data acquired with this sequence are Fourier transformed and phase corrected in a manner similar to that described earlier (*7, 14*), with the only difference being the shearing transformation described in the previous section. This shearing transformation may be accomplished by applying the phase correction of Eq. [6] to the complex 2D data assembled from the hypercomplex data after the Fourier transform in $t_2$.

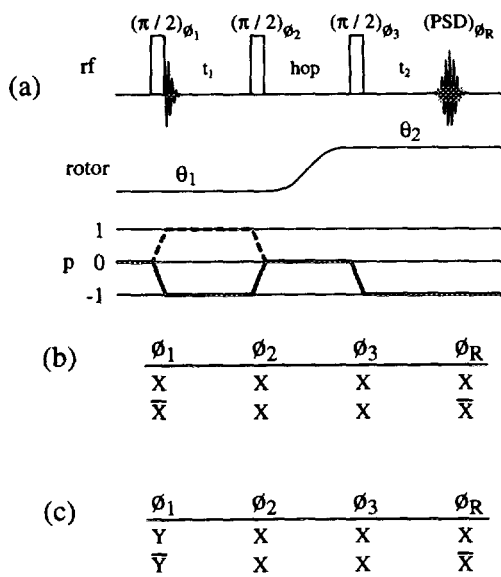


FIG. 3. (a) Pulse sequence for hypercomplex dynamic-angle spinning. (b) RF pulse phase cycle for the real part of $t_1$ evolution. (c) RF pulse phase cycle for the imaginary part of $t_1$ evolution.

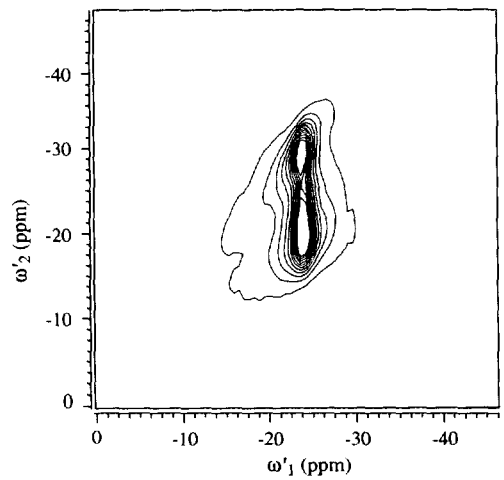


FIG. 4. Pure-absorption-mode 2D DAS $^{87}$Rb NMR spectrum of $RbClO_4$ taken at 11.7 T using the pulse sequence in Fig. 3. The contour plot was calculated using 16 equally spaced contour levels over a range of −30 to 70% of the maximum peak. Negative contours are shown in gray. Additional experimental details are given in Table 1.

The overall signal-to-noise ratio of the 2D spectrum will be directly related to the 2D time-domain signal amplitude at ($t_1 = 0, t_2 = 0$), since this point corresponds to a projection over both $\omega_1$ and $\omega_2$ in the 2D spectrum (*16*). The 2D hypercomplex DAS experiment described in Fig. 3 has the same value for the time-domain signal amplitude at ($t_1 = 0, t_2 = 0$) as the original DAS experiment in Fig. 1a. Because the hypercomplex DAS experiment in Fig. 3 employs phase separation in $t_1$, however, it has a $2^{1/2}$ increase in sensitivity over the original DAS (*6*).

An experimental example of a 2D DAS spectrum of $^{87}RbClO_4$ obtained with the hypercomplex pulse sequence in Fig. 3 and sheared using the phase correction of Eq. [6] is shown in Fig. 4. This 2D DAS spectrum appears in pure absorption mode and, as seen in Table 1, has a signal-to-noise ratio greater by a factor of $\sim 2^{1/2}$ than that of a 2D DAS spectrum (not shown) obtained using the pulse sequence in Fig. 1a.

It is interesting to note that although the 2D spectra associated with the echo and antiecho pathways are each mixed

phase and have the same intensity for the time-domain signal amplitude at ($t_1 = 0, t_2 = 0$) as the original and hypercomplex DAS experiment, there are interference effects in the 2D lineshapes from the inhomogeneous broadening (*7*) that result in a sensitivity for the 2D echo spectrum higher than that for the antiecho spectrum. This may be understood by considering, as an example, inhomogeneous Lorentzian broadening of the 2D echo and antiecho signals having the form

$$S_E(t_1, t_2) = e^{-\lambda^+|t_2 - t_1|}e^{-\lambda(t_1+t_2)} \quad [8]$$

and

$$S_A(t_1, t_2) = e^{-\lambda^+|t_2 + t_1|}e^{-\lambda(t_1+t_2)}, \quad [9]$$

where $S_E(t_1, t_2)$ and $S_A(t_1, t_2)$ are the echo and antiecho signals, $\lambda^+$ is the inhomogeneous Lorentzian broadening, and $\lambda$ is the homogeneous Lorentzian broadening. A Fourier transform of $S_E(t_1, t_2)$ and $S_A(t_1, t_2)$ with respect to $t_2$ gives

$$S_E(t_1, \omega_2) = \{[A(\omega_2) - A'(\omega_2)] - i[D(\omega_2) - D'(\omega_2)]\}e^{-2\lambda t_1}e^{i\omega_2 t_1} + [A'(\omega_2) - iD'(\omega_2)]e^{-(\lambda+\lambda^+)t_1} \quad [10]$$

and

$$S_A(t_1, \omega_2) = [A'(\omega_2) - iD'(\omega_2)]e^{-(\lambda+\lambda^+)t_1}, \quad [11]$$

where

$$A(\omega) = \frac{\lambda + \lambda^+}{(\lambda + \lambda^+)^2 + \omega^2}, \quad [12]$$

$$D(\omega) = \frac{\omega}{(\lambda + \lambda^+)^2 + \omega^2} \quad [13]$$

and

$$A'(\omega) = \frac{\lambda - \lambda^+}{(\lambda - \lambda^+)^2 + \omega^2}, \quad [14]$$

$$D'(\omega) = \frac{\omega}{(\lambda - \lambda^+)^2 + \omega^2}. \quad [15]$$

In DAS where $\lambda^+ \gg \lambda$, one finds $A'(\omega) = -A(\omega)$ and $D'(\omega) = D(\omega)$, and Eq. [10] simplifies to

$$S_E(t_1, \omega_2) = 2A(\omega_2)e^{-2\lambda t_1}e^{i\omega_2 t_1} + [A'(\omega_2) - iD'(\omega_2)]e^{-(\lambda+\lambda^+)t_1}. \quad [16]$$

For large inhomogeneous broadenings and large $t_1$ times, the second term in Eq. [16] may be neglected and the Fourier transform of the echo signal is pure absorption mode (*8*), while the antiecho signal is still mixed phase. The 2D echo spectrum will not be completely pure absorption mode, however, because of the dispersion-mode components present when $t_1$ is near zero. As the inhomogeneous broadening becomes larger with respect to the homogeneous broadening, the 2D echo spectrum intensity increases over the 2D antiecho spectrum intensity, and the 2D echo lineshape contains more absorption-mode than dispersion-mode character. Ultimately, as $\lambda^+/\lambda \to \infty$, the 2D echo spectrum has a signal-to-noise ratio a factor of $2^{1/2}$ better than that of the pure-absorption-mode 2D spectrum obtained using the hypercomplex experiment in Fig. 3.

TABLE 1

Experimentally Measured Signal-to-Noise Ratios of 2D DAS $^{87}$Rb NMR Spectra of $RbClO_4$ Obtained at 163.6 MHz with Various DAS Pulse Sequences

| Sequence | Ref. | Pure phase | *S/N* |
|---|---|---|---|
| *z*-Filter DAS | *5* | Yes | 15.8 |
| DAS | *1, 3* | No | 20.6 |
| Hypercomplex DAS | This work (Fig. 3) | Yes | 31.3 |
| Echo DAS | This work (Fig. 2a) | No | 31.6 |
| Antiecho DAS | This work | No | 10.9 |
| Shifted-echo DAS | This work (Fig. 6) | Yes | 43.4 |
| Hypercomplex shifted-echo DAS | This work (Fig. 7) | Yes | 67.0 |

*Note.* All spectra were recorded in about eight hours with a recycle time of 1.6 s, 128 transients averaged for each $t_1$ time, and a digital resolution of 78.1 Hz in $\omega_2'$ and 156.3 Hz in $\omega_1'$, using the DAS angle pair (0°, 63.4°) with a hopping time of 50 ms. In both shifted-echo experiments, the echoes were shifted in $t_2$ by 900 $\mu$s. A second hop to the magic angle (54.7°) was not implemented in the *z*-filter DAS experiment to facilitate comparison with the other sequences. A *z*-filter delay of 11 ms was employed. Each 2D data set was apodized as outlined in the text with a 200 Hz Gaussian broadening applied in the $\omega_2$ dimension.

Combining the hypercomplex 2D DAS data obtained with the pulse sequence in Fig. 3 to select the $p = 0 \to -1 \to 0 \to -1$ pathway yields the DAS echo signal. After Fourier transformation and shearing with the phase correction of Eq. [7], the 2D DAS spectrum shown in Fig. 5 is obtained. Because of the interference effects of inhomogeneous broadenings, this 2D DAS spectrum appears in almost pure absorption mode and, as seen in Table 1, has a signal-to-noise similar to that of the 2D DAS spectrum in Fig. 4 obtained using the hypercomplex pulse sequence in Fig. 3. Combining the hypercomplex 2D DAS data obtained with the pulse sequence in Fig. 3 to select the $p = 0 \to +1 \to 0 \to -1$ pathway yields the DAS antiecho signal. The signal-to-noise ratio for the anisotropic antiecho spectrum (not shown) is also given in Table 1. As expected, the antiecho signal-to-noise ratio is much lower than that of the echo signal.

It should be mentioned that, although in this case the mixed-phase 2D echo pathway DAS spectrum has a signal-to-noise similar to that of the pure-absorption-mode 2D spectrum obtained with the hypercomplex DAS approach,

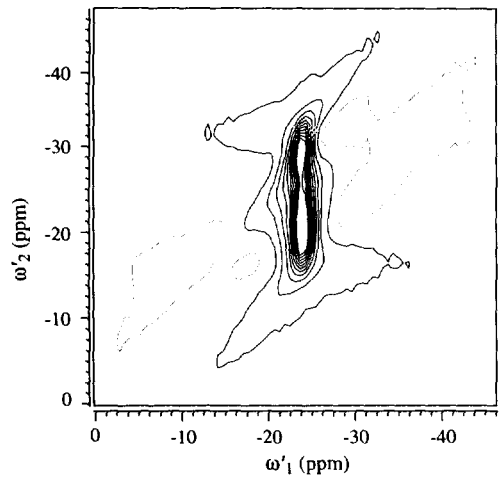


FIG. 5. Mixed-phase 2D DAS $^{87}$Rb NMR spectrum of $RbClO_4$ taken at 11.7 T using the pulse sequence in Fig. 2a. The contour plot was calculated using 16 equally spaced contour levels over a range of −30 to 70% of the maximum peak. Negative contours are shown in gray. The small amount of dispersion-mode character is a result of not being able to obtain a complete echo during $t_2$ for the shorter values of $t_1$. Additional experimental details are given in Table 1.

in general the projection onto the isotropic axis of the mixed-phase 2D echo spectrum will have a signal-to-noise factor of $2^{1/2}$ greater than that of the same projection of the pure-phase 2D spectrum obtained with the hypercomplex approach in Fig. 4.

*Shifted-Echo DAS*

The dispersion-mode components present in the inhomogeneously broadened 2D echo spectrum in Fig. 5 may be suppressed by time shifting the coherence-transfer echoes formed because of the inhomogeneous broadening. In DAS this can be accomplished by using a $\pi$ pulse to shift the DAS echo in $t_2$ by an amount $\tau$ so that an entire echo is obtained in $t_2$ for all values of $t_1$, including $t_1 = 0$. Again using the example of inhomogeneous Lorentzian broadening, the time-shifted 2D echo signal is

$$S_E(t_1, t_2) = e^{-\lambda^+|t_2 - t_1 - \tau|} e^{-\lambda(t_1 + t_2 + \tau)}, \quad [17]$$

and the Fourier transform with respect to $t_2$, assuming $\lambda^+ \gg \lambda$, gives

$$S_E(t_1, \omega_2, \tau) = 2A(\omega_2) e^{-2\lambda(t_1+\tau)} e^{-i\omega_2(t_1+\tau)} + [A'(\omega_2) - iD'(\omega_2)] e^{-(\lambda+\lambda^+)(t_1+\tau)}. \quad [18]$$

When $\tau$ is large enough that the second term can be neglected, a pure-absorption-mode spectrum is obtained that has a signal-to-noise factor of $2^{1/2} e^{-2\lambda\tau}$ better than that of the hypercomplex approach.

The pulse sequence and phase cycle for the shifted-echo approach to pure-phase DAS are described in Fig. 6. The length of $\tau$ is a multiple of the rotor period, and typically half the width of the echo, so that the signal in $t_2$ begins at zero. The complex 2D data acquired with this sequence are processed in the same fashion as conventional phase-modulated 2D data, with the only differences being a $\tau$-dependent first-order phase correction of

$$\phi(\tau, \omega_2) = \omega_2 \tau \quad [19]$$

to remove the phase modulation because of the time-shifted echo and the $t_1$-dependent first-order correction of Eq. [7] to perform the shearing transformation. Both are applied after the Fourier transform with respect to $t_2$. Using the pulse sequence in Fig. 6, a pure-absorption-mode 2D DAS spectrum of $^{87}RbClO_4$ was obtained (not shown) and, as seen in Table 1, the signal-to-noise is a factor of $\sim 2^{1/2}$ better than that of the hypercomplex DAS experiment of Fig. 3 and a factor of $\sim 2$ better than those of the original mixed-phase and $z$-filtered pure-phase DAS experiments.

A potential difficulty with this approach is that $\tau$ must be adjusted to be large enough to obtain the whole echo signal. Truncating the echo on either side of its maximum will add dispersion-mode components into the 2D spectrum. However, if the homogeneous broadening is so large that

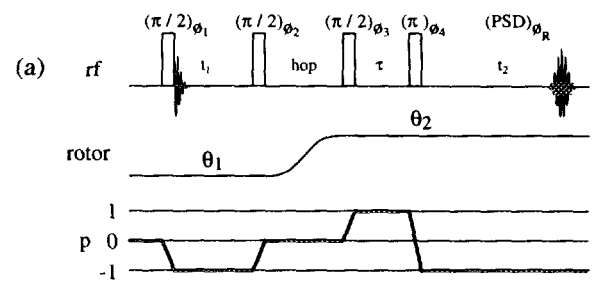


(b)

| ø1 | ø2 | ø3 | ø4 | øR |
|---|---|---|---|---|
| X | X | X | X | X |
| Y | X | X | X | Y |
| $\bar{X}$ | X | X | X | $\bar{X}$ |
| $\bar{Y}$ | X | X | X | $\bar{Y}$ |
| X | X | Y | X | $\bar{Y}$ |
| Y | X | Y | X | X |
| $\bar{X}$ | X | Y | X | Y |
| $\bar{Y}$ | X | Y | X | $\bar{X}$ |
| X | X | $\bar{X}$ | X | $\bar{X}$ |
| Y | X | $\bar{X}$ | X | $\bar{Y}$ |
| $\bar{X}$ | X | $\bar{X}$ | X | X |
| $\bar{Y}$ | X | $\bar{X}$ | X | Y |
| X | X | $\bar{Y}$ | X | Y |
| Y | X | $\bar{Y}$ | X | $\bar{X}$ |
| $\bar{X}$ | X | $\bar{Y}$ | X | $\bar{Y}$ |
| $\bar{Y}$ | X | $\bar{Y}$ | X | X |

FIG. 6. (a) Pulse sequence for shifted-echo dynamic-angle spinning. (b) RF pulse phase cycle for (a).

$$e^{-2\lambda\tau} \leqslant 1/2^{1/2}, \qquad [20]$$

then the hypercomplex DAS sequence in Fig. 3 should be the preferred approach.

It is interesting to note that since whole-echo acquisition results in only absorption-mode spectra in $\omega_2$, it is not necessary to include both $p = \pm 1$ coherence pathways in $t_1$ to obtain a pure-absorption-mode 2D DAS spectrum. This is because whole-echo acquisition in $t_2$ provides a means of obtaining both $p = \pm 1$ coherence pathways in $t_2$ for a single pathway in $t_1$.

*Hypercomplex and Shifted-Echo DAS*

While the shifted-echo approach to pure-phase DAS provides up to a factor of 2 enhancement in sensitivity over the original mixed-phase DAS experiment, there are certain situations where an additional factor of $2^{1/2}$ enhancement can be obtained by combining phase separation in $t_1$ with shifting the echo in $t_2$. This approach amounts to whole-echo acquisition of both the echo and the antiecho DAS signals and is practical only when there is an additional inhomogeneous broadening associated with the isotropic dimension. This often occurs when DAS is applied to materials in which there is a continuous distribution of atomic environments resulting in a continuous distribution of second-order quadrupolar or chemical shifts (*17*). Again using an example of inhomogeneous Lorentzian broadening, the time-shifted 2D echo and antiecho signals may be written

$$S_E(t_1, t_2) = e^{-i(\lambda^+ + \lambda^0)t_2 - (\lambda^+ + \lambda^0)\tau - (\lambda^+ - \lambda^0)t_1 |} e^{-\lambda(t_1 + t_2 + \tau)}, \qquad [21]$$

$$S_A(t_1, t_2) = e^{-i(\lambda^+ + \lambda^0)t_2 - (\lambda^+ + \lambda^0)\tau + (\lambda^+ - \lambda^0)t_1 |} e^{-\lambda(t_1 + t_2 + \tau)}, \qquad [22]$$

where $\lambda^0$ is the inhomogeneous broadening in the isotropic dimension. The Fourier transform with respect to $t_2$ assuming $\lambda^+ \geqslant \lambda^0 \gg \lambda$ gives

$$\begin{aligned} S_E(t_1, \omega_2) &= ZA(\omega_2) e^{-2\lambda\tau} e^{-i\omega_2\tau} e^{-[(2\lambda\lambda^+/(\lambda^+ + \lambda^0)]t_1} e^{-i\omega_2[(\lambda^+ - \lambda^0)/(\lambda^+ + \lambda^0)]t_1} \\ &\quad + [A(\omega_2) - iD(\omega_2)] e^{-(\lambda + \lambda^+ + \lambda^0)\tau} e^{-(\lambda^+ - \lambda^0 + \lambda)t_1}, \end{aligned} \qquad [23]$$

$$\begin{aligned} S_A(t_1, \omega_2) &= ZA(\omega_2) e^{-2\lambda\tau} e^{-i\omega_2\tau} e^{-[2\lambda\lambda^0/(\lambda^+ + \lambda^0)]t_1} e^{i\omega_2[(\lambda^+ - \lambda^0)/(\lambda^+ + \lambda^0)]t_1} \\ &\quad + [A(\omega_2) - iD(\omega_2)] e^{-(\lambda + \lambda^+ + \lambda^0)\tau} e^{-(\lambda^+ - \lambda^0 - \lambda)t_1}, \end{aligned} \qquad [24]$$

where

$$A(\omega) = \frac{\lambda^+ + \lambda^0}{(\lambda^+ + \lambda^0)^2 + \omega^2}, \qquad [25]$$

$$D(\omega) = \frac{\omega}{(\lambda^+ + \lambda^0)^2 + \omega^2}. \qquad [26]$$

In order to ensure pure-absorption-mode 2D spectra and no truncation artifacts it is necessary to shift both echo and antiecho signals far enough into $t_2$ that the second terms in Eqs. [23] and [24] can be neglected for all values of $t_1$.

The pulse sequence and phase cycle for the combined hypercomplex and shifted-echo approach to pure-phase DAS are described in Fig. 7. The length of $\tau$ is a multiple of the rotor period and is approximated by

$$\tau \approx \tau' + \left(\frac{\lambda^+ - \lambda^0}{\lambda^+ + \lambda^0}\right)\left(\frac{x_2}{x_1}\right) t_1^{\max}, \qquad [27]$$

where $\tau'$ is typically half the width of the echo, so that the signal in $t_2$ begins at zero for $t_1 = 0$, and $t_1^{\max}$ is determined by the desired resolution in the $\omega_1$ domain. However, if the homogeneous broadenings are so large that

$$e^{-2\lambda\tau} \leqslant 1/2^{1/2}, \qquad [28]$$

then either the shifted-echo or the hypercomplex DAS experiments should be the preferred approach.

With the exception of the time-domain filters (see the next section) and the phase corrections, the hypercomplex 2D

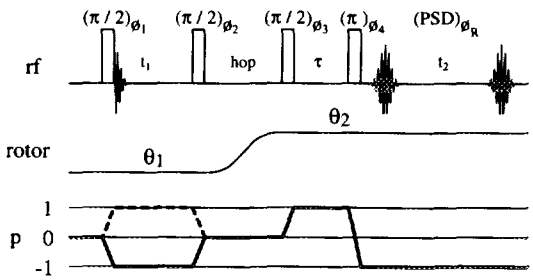


(b)

| $\phi_1$ | $\phi_2$ | $\phi_3$ | $\phi_4$ | $\phi_R$ |
|---|---|---|---|---|
| X | X | X | X | X |
| $\bar{X}$ | X | X | X | $\bar{X}$ |
| X | X | Y | X | $\bar{Y}$ |
| $\bar{X}$ | X | Y | X | Y |
| X | X | $\bar{X}$ | X | $\bar{X}$ |
| $\bar{X}$ | X | $\bar{X}$ | X | X |
| X | X | $\bar{Y}$ | X | Y |
| $\bar{X}$ | X | $\bar{Y}$ | X | $\bar{Y}$ |

(c)

| $\phi_1$ | $\phi_2$ | $\phi_3$ | $\phi_4$ | $\phi_R$ |
|---|---|---|---|---|
| Y | X | X | X | X |
| $\bar{Y}$ | X | X | X | $\bar{X}$ |
| Y | X | Y | X | $\bar{Y}$ |
| $\bar{Y}$ | X | Y | X | Y |
| Y | X | $\bar{X}$ | X | $\bar{X}$ |
| $\bar{Y}$ | X | $\bar{X}$ | X | X |
| Y | X | $\bar{Y}$ | X | Y |
| $\bar{Y}$ | X | $\bar{Y}$ | X | $\bar{Y}$ |

FIG. 7. (a) Pulse sequence for combined shifted-echo and hypercomplex dynamic-angle spinning. (b) RF pulse phase cycle for the real part of $t_1$ evolution. (c) RF pulse phase cycle for the imaginary part of $t_1$ evolution.

data acquired with this sequence are processed in a fashion similar to that of conventional hypercomplex 2D data. The $\tau$-dependent first-order phase correction of

$$\phi(\tau, \omega_2) = \omega_2\tau \qquad [29]$$

is applied to the hypercomplex 2D data after the Fourier transform with respect to $t_2$ to remove the phase modulation from the time-shifted echo. The $t_1$-dependent first-order phase correction of Eq. [7] is applied to the complex 2D data assembled from the hypercomplex data after the $\tau$-dependent first-order phase correction to perform the shearing transformation.

Although there is no significant inhomogeneous broadening in the isotropic dimension of the $^{87}RbClO_4$ 2D DAS spectrum, a 2D spectrum was obtained (not shown) using the pulse sequence in Fig. 7 to compare the sensitivity of this approach to that of the other DAS pulse sequences. Despite the minor truncation of the antiecho signal, the signal-to-noise ratio listed in Table 1 is a factor of $\sim 2^{1/2}$ better than that of the shifted-echo DAS experiment in Fig. 6, a factor of $\sim 2$ better than that of the hypercomplex DAS experiment in Fig. 3, and a factor of $\sim 8^{1/2}$ better than those of the original mixed-phase and $z$-filtered pure-phase DAS experiments.

## 2D TIME-DOMAIN FILTER FUNCTIONS

In general, the optimum 2D weighting function, $h(t_1, t_2)$, for enhancing the signal-to-noise of a 2D spectrum will depend on the particular coherence-transfer pathway for the 2D experiment. When there are large inhomogeneous broadenings, this presents a complication for hypercomplex 2D data where the time-domain signal consists of the sum and difference of the signals for the echo, $S_E(t_1, t_2)$, and antiecho, $S_A(t_1, t_2)$, signals. The 2D hypercomplex time-domain signal may be written (*7*)

$$^4S(t_1, t_2) = S_C(t_1, t_2) + jS_S(t_1, t_2), \qquad [30]$$

where

$$S_C(t_1, t_2) = \frac{1}{2}\{S_E(t_1, t_2) + S_A(t_1, t_2)\} \qquad [31]$$

and

$$S_S(t_1, t_2) = -\frac{i}{2}\{S_E(t_1, t_2) - S_A(t_1, t_2)\} \qquad [32]$$

are the cosine and sine amplitude-modulated 2D time-domain signals, and $i$ and $j$ are two independent imaginary units which refer to the two orthogonal axes,

$$i^2 = j^2 = -1. \qquad [33]$$

For inhomogeneously broadened systems, the optimum 2D weighting functions for the echo and antiecho pathways, when using a Lorentzian broadening of $\lambda_h$, are

$$h_E(t_1, t_2) = e^{-\lambda_h|t_2 - t_1|} \qquad [34]$$

and

$$h_A(t_1, t_2) = e^{-\lambda_h|t_2 + t_1|} \qquad [35]$$

respectively. The properly weighted echo and antiecho signals are thus

$$S_E^h(t_1, t_2) = S_E(t_1, t_2)h_E(t_1, t_2) \qquad [36]$$

and

$$S_A^h(t_1, t_2) = S_A(t_1, t_2)h_A(t_1, t_2) \qquad [37]$$

and therefore the properly weighted cosine and sine signals are

$$S_C^h(t_1, t_2) = \frac{1}{2}\{S_E(t_1, t_2)h_E(t_1, t_2) + S_A(t_1, t_2)h_A(t_1, t_2)\} \qquad [38]$$

and

$$S_S^h(t_1, t_2) = \frac{-i}{2}\{S_E(t_1, t_2)h_E(t_1, t_2) - S_A(t_1, t_2)h_A(t_1, t_2)\}. \qquad [39]$$

Clearly a single time-domain filter function for the cosine or sine data cannot be factored out. Thus in order to apply the optimum time-domain filter to hypercomplex data, it is first necessary to separate the 2D hypercomplex time-domain signal into the echo and antiecho complex 2D time-domain signals, where the different optimum filters for the echo and antiecho signals can then be properly applied. The 2D echo and antiecho time-domain signals can be obtained from the cosine- and sine-modulated 2D signals using

$$S_E(t_1, t_2) = S_C(t_1, t_2) + iS_S(t_1, t_2) \qquad [40]$$

and

$$S_A(t_1, t_2) = S_C(t_1, t_2) - iS_S(t_1, t_2) \qquad [41]$$

An echo envelope with an exponential or Gaussian decay centered about the shifting echo or antiecho signal maximum

as a time-domain filter function should provide an optimum sensitivity enhancement. After filtering, the 2D echo and antiecho time-domain signals, $S_E(t_1, t_2)$ and $S_A(t_1, t_2)$, may then be converted back to the 2D hypercomplex time-domain signal according to Eqs. [31] and [32] and processed as usual.

## PHASE SPECTRUM CORRECTION

While in principle Eq. [19] or [29] should provide the necessary first-order phase correction to remove the phase modulation because of the time-shifted echo, in practice it can be difficult to find the optimal zero- and first-order phase corrections. This is especially true when the 2D spectrum contains many lines.

An advantage of the shifted-echo sequences in Figs. 6 and 7 is that an entire echo is collected in $t_2$ for all values of $t_1$, including $t_1 = 0$. Because the echo acquired for $t_1 = 0$ will contain no modulation from $t_1$ evolution, its Fourier transform should be completely real after the phase correction of Eq. [19] or [29] is applied:

$$A(t_1 = 0, \omega_2) = e^{i\phi(\tau,\omega_2)} S'(t_1 = 0, \omega_2). \quad [42]$$

Assuming that $A(t_1 = 0, \omega_2)$ contains no negative peaks, the simple relation

$$A(t_1 = 0, \omega_2) = \sqrt{S_R(t_1 = 0, \omega_2)^2 + S_I(t_1 = 0, \omega_2)^2}, \quad [43]$$

where $S_R(t_1 = 0, \omega_2)$ and $S_I(t_1 = 0, \omega_2)$ are the real and imaginary parts, respectively, of $S(t_1 = 0, \omega_2)$, can be used to obtain the phase spectrum, $\Phi(\omega_2)$, defined by

$$\Phi(\omega_2) = \cos^{-1}\left[\frac{S_R(t_1 = 0, \omega_2)}{A(t_1 = 0, \omega_2)}\right], \quad [44]$$

$$\Phi(\omega_2) = \sin^{-1}\left[\frac{S_I(t_1 = 0, \omega_2)}{A(t_1 = 0, \omega_2)}\right]. \quad [45]$$

Instead of Eqs. [19] or [29], the phase spectrum $\Phi(\omega_2)$ can be used to phase correct the 2D spectrum after the Fourier transform in $t_2$. Thus, it is not necessary to interactively phase correct the $t_1 = 0$ cross section, $S(t_1 = 0, \omega_2)$, when it is a Fourier transform of an entire echo. For hypercomplex data, the cosine $t_1 = 0$ cross section $S_C(t_1 = 0, \omega_2)$ is used to phase correct both the cosine and the sine halves of the hypercomplex 2D data. A limitation of this method is that the signal-to-noise of the $t_1 = 0$ cross section must be high enough that noise in the phase spectrum does not introduce significant distortions of the 2D lineshapes. This simple phasing technique is not limited to DAS but is applicable to any 2D experiment that employs whole-echo acquisition, which should always be possible when a correlation with an inhomogeneously broadened dimension is involved.

## ANALYSIS OF ANISOTROPIC LINESHAPES

In order to extract the anisotropic quadrupolar tensor parameters from the 2D DAS spectrum it is necessary that singularities in the anisotropic lineshape be well defined. As pointed out by Mueller *et al.* (*5*), this may be a problem when the final angle for detection is not the magic angle (54.74°), because the broadenings from dipolar couplings and CSA may obscure the structure in the anisotropic lineshape and lead to poorly defined singularities. Unfortunately, 54.74° is not a solution of Eqs. [4] and [5]. One approach, described by Mueller *et al.* (*5*), is to incorporate a second hop during the $z$ filter of their pure-absorption-mode sequence so that detection can occur at any angle, independent of Eqs. [4] and [5]. Using 54.74° as the detection angle, an anisotropic dimension containing only fourth-rank anisotropies and thus well-resolved singularities can be obtained. Unfortunately, as mentioned earlier, the second storage and recall pulses required for the $z$ filter and second hop come at a loss of $2^{1/2}$ in sensitivity. A compromise that recovers this factor of $2^{1/2}$ is to eliminate the $z$ filter and second hop and find the DAS angle pair where the ratio of fourth-rank to second-rank anisotropies is greatest. With this angle pair there will still be second-rank broadenings but their effects will be minimized. Figure 8 is a plot of the ratio of fourth-rank to second-rank anisotropies versus $\theta$. As can be seen from the figure, the value of $\theta = 0°$, or the (0°, 63.43°) angle pair, is optimal. Using the (0°, 63.43°) angle pair, the ratio of fourth-rank to second-rank anisotropies is increased by a factor of 1.8 over the ratio of the (37.38°, 79.19°) DAS angle pair. The (0°, 63.43°) angle pair also has the additional advantage that the spinning sidebands in the $\omega_1'$ dimension appear at 83% of the actual spinning speed instead of 50% for the (37.38°, 79.19°) DAS angle pair (*13*).

Using the shifted-echo DAS sequence in Fig. 7 with the DAS angle pair (0°, 63.43°), a pure-absorption-mode 2D DAS spectra of $^{87}RbNO_3$ was obtained and processed using the time-domain filter function and the phase spectrum correction described earlier. The 2D DAS spectrum is shown in Fig. 9. $RbNO_3$ has three crystallographically distinct Rb sites and the projection onto $\omega_1'$ clearly resolves all sites (*18*).

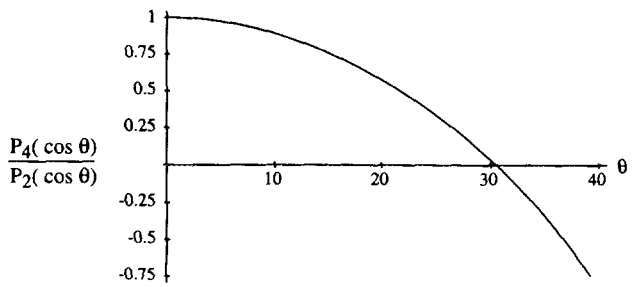


FIG. 8. Ratio of Legendre polynomials $P_4(\cos\theta)$ and $P_2(\cos\theta)$ as a function of $\theta$.

Just as in Fig. 4, this 2D spectrum does not contain any of the dispersive character found in the lineshapes in Figs. 1b and 2b. The anisotropic lineshapes shown in Fig. 9 were fitted using a least-squares procedure to obtain the quadrupolar and chemical-shift parameters listed in Table 2. Simulations obtained from the best-fit parameters are also shown along with the experimental lineshapes in Fig. 9.

TABLE 2

**$^{87}$Rb Quadrupolar Coupling and Chemical-Shift Parameters for $RbNO_3$ Obtained from the Least-Squares Analysis of the Separated Anisotropic Lineshapes Taken from the 2D DAS Spectrum Shown in Fig. 9**

| Site | $C_q$ (MHz) | $\eta_q$ | $\sigma_{iso,CS}$ (ppm) |
|---|---|---|---|
| 1 | 1.6 | 0.29 | −29.4 |
| 2 | 1.7 | 0.56 | −31.4 |
| 3 | 2.1 | 0.71 | −28.4 |

## EXPERIMENTAL

$RbClO_4$ and $RbNO_3$ were obtained from Aldrich and used without further purification. All spectra are referenced relative to aqueous 1 *M* $RbNO_3$ as an external frequency standard. The DAS angle pair used in all experiments was (0°, 63.43°). All experiments on $RbClO_4$ were performed at 11.7 T using a DAS probe described elsewhere (*19*). All experiments on $RbNO_3$ were performed at 4.22 T using a previously described DAS probe (*20*) that was modified by changing the RF coil to a loop–gap resonator instead of a solenoid so NMR transitions could be excited and detected while spinning about an angle of 0° with respect to the magnetic field. The anisotropic lineshapes were fitted using a least-squares procedure to obtain the quadrupolar and chemical-shift parameters.

## SUMMARY

We have described new approaches for the dynamic-angle spinning experiment that provide pure-absorption-mode 2D DAS spectra with improved sensitivity so the experiment time can now be reduced by up to a factor of 8 from that of previous 2D DAS experiments. In one approach, the evolution times in the DAS experiment are redefined so the hypercomplex approach to pure-phase 2D NMR can be combined with a shearing transformation to obtain a pure-absorption-mode 2D DAS spectrum. In another approach, the coherence-transfer echoes, which are formed because of the inhomogeneous broadenings intrinsic to the DAS experiment, are time shifted with a $\pi$ pulse to obtain whole-echo acquisition, and thus a pure-absorption-mode 2D spectrum. When there is an inhomogeneous broadening associated with the isotropic DAS dimension, these two approaches can be combined into a single approach for a sensitivity higher than that of the individual approaches. We also outline a procedure for applying the optimum time-domain filter function to hypercomplex data, where signals from different coherence-transfer pathways are present in the same data. Finally, a simple noninteractive phase-correction technique is described that uses the $t_1 = 0$ coherence-

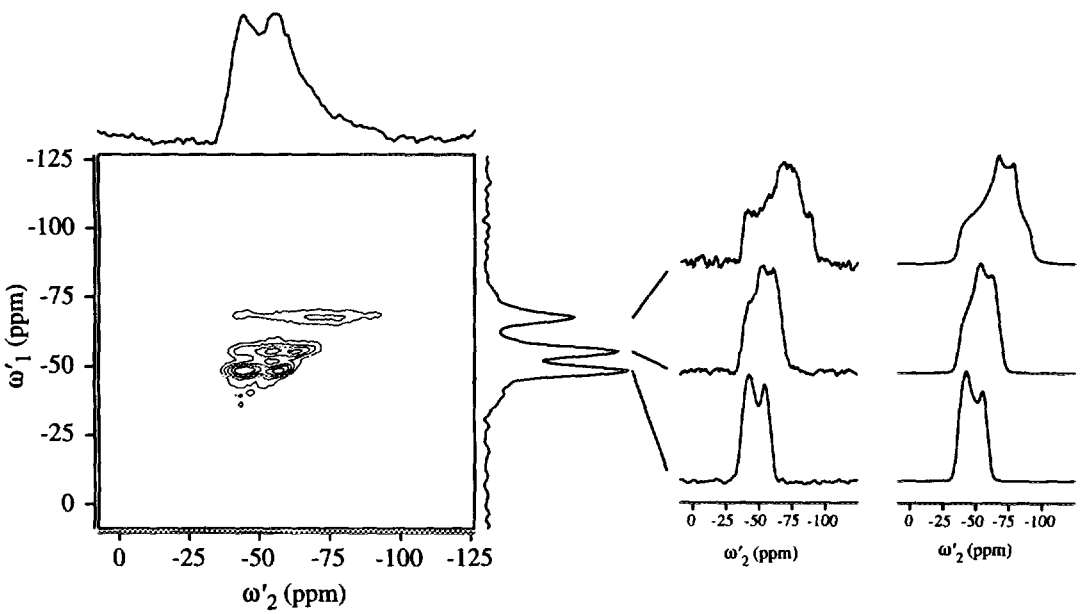


FIG. 9. Two-dimensional DAS $^{87}$Rb NMR spectrum of $RbNO_3$ taken at 11.7 T using the sequence in Fig. 6 with the DAS angle pair (0°, 63.43°). Also shown are cross sections from the two-dimensional DAS spectrum taken parallel to the $\omega_2$ (63.43°) axis for the three sites in $RbNO_3$. "Best-fit" simulations of the three sites are shown alongside each cross section. Best-fit quadrupolar and chemical-shift parameters are listed in Table 2.

transfer echo to provide a spectrum of phase corrections that can be used to obtain a positive pure-absorption-mode 2D spectrum. The techniques described here to obtain and process pure-absorption-mode 2D DAS spectra should be applicable to other 2D NMR experiments that involve correlations with inhomogeneously broadened spectra.

## ACKNOWLEDGMENTS

We thank Lyndon Emsley for helpful discussions. This investigation was supported by the Director, Office of Energy Research, Office of Basic Energy Sciences, Materials Sciences Division, and Office of Health and Environmental Research, Health Effects Research Division of the U.S. Department of Energy under Contract DE-AC03-76SF00098. M.A.E. and P.J.G. were supported by National Institutes of Health, National Research Service Awards from the National Institute of General Medical Sciences. A.L. acknowledges financial support from the Commissariat à l'Energie Atomique, France, and from the North-Atlantic Treaty Organization (Grant 68C89FR). J.H.B. was supported by a NSF graduate fellowship. U.W. was supported by a Feodor Lynen fellowship of the Alexander von Humboldt Foundation.

## REFERENCES

1. A. Llor and J. Virlet, *Chem. Phys. Lett.* **152,** 248 (1988).
2. B. F. Chmelka, K. T. Mueller, A. Pines, J. Stebbins, Y. Wu, and J. W. Zwanziger, *Nature* **339,** 42 (1989).
3. K. T. Mueller, B. Q. Sun, G. C. Chingas, J. W. Zwanziger, T. Terao, and A. Pines, *J. Magn. Reson.* **86,** 470 (1990).
4. K. T. Mueller, Y. Wu, B. F. Chmelka, J. Stebbins, and A. Pines, *J. Am. Chem. Soc.* **113,** 32 (1991).
5. K. T. Mueller, E. W. Wooten, and A. Pines, *J. Magn. Reson.* **92,** 620 (1991).
6. J. Keeler and D. Neuhaus, *J. Magn. Reson.* **63,** 454 (1985).
7. R. R. Ernst, G. Bodenhausen, and A. Wokaun, "Principles of Nuclear Magnetic Resonance in One and Two Dimensions," Oxford Univ. Press, New York/London, 1987.
8. A. Bax, A. F. Mehlkopf, and J. Smidt, *J. Magn. Reson.* **35,** 373 (1979).
9. K. Nagayama, A. Kumar, K. Wüthrich, and R. R. Ernst, *J. Magn. Reson.* **40,** 321 (1980).
10. G. Wider, S. Macura, A. Kumar, R. R. Ernst, and K. Wüthrich, *J. Magn. Reson.* **56,** 207 (1984).
11. A. C. Kolbert, M. H. Levitt, and R. G. Griffin, *J. Magn. Reson.* **85,** 42 (1989).
12. K. Nagayama, P. Bachmann, K. Wüthrich, and R. R. Ernst, *J. Magn. Reson.* **31,** 133 (1978).
13. P. J. Grandinetti, Y. K. Lee, J. H. Baltisberger, B. Q. Sun, and A. Pines, *J. Magn. Reson. Ser. A* **102,** 195 (1993).
14. D. J. States, R. A. Haberkorn, and D. J. Ruben, *J. Magn. Reson.* **48,** 286 (1982).
15. G. Drobny, A. Pines, S. Sinton, D. P. Weitekamp, and D. Wemmer, *Symp. Faraday Soc.* **13,** 93 (1980).
16. M. H. Levitt, G. Bodenhausen, and R. R. Ernst, *J. Magn. Reson.* **58,** 462 (1984).
17. I. Farnan, P. J. Grandinetti, J. H. Baltisberger, J. F. Stebbins, U. Werner, M. A. Eastman, and A. Pines, *Nature* **358,** 31 (1992).
18. J. H. Baltisberger, S. L. Gann, E. W. Wooten, T. H. Chang, K. T. Mueller, and A. Pines, *J. Am. Chem. Soc.*, **114,** 7489 (1992).
19. K. T. Mueller, G. C. Chingas, and A. Pines, *Rev. Sci. Instrum.* **62,** 1445 (1991).
20. M. A. Eastman, P. J. Grandinetti, Y. K. Lee, and A. Pines, *J. Magn. Reson.* **98,** 333 (1992).